Late-Holocene dynamics of sea-surface temperature and terrestrial hydrology in southwestern Africa

Robyn Granger,[1] Michael E Meadows,[1,2] Annette Hahn,[3]
Matthias Zabel,[3] Jan-Berend W Stuut,[3,4] Nicole Herrmann[3,5]
and Enno Schefuß[3]

Abstract

Southwest Africa is an important region for paleo-climatic studies, being influenced by both tropical and temperate climate systems and thus reflecting the interplay of variable controls. The aim of this study was to unravel the interaction of sea-surface temperature (SST) changes in the southernmost Benguela upwelling system with precipitation changes in South Africa's winter rainfall zone (WRZ) during the late Holocene. Therefore, a marine sediment core from the southernmost Benguela upwelling system was investigated to reconstruct climate changes in this region for the past ~2000 years. Grain size and geochemical analyses were conducted to reconstruct changes in fluvial sediment discharge and weathering intensity, while SST changes were estimated using alkenone paleo-thermometry. Results show that the southernmost Benguela behaves distinctly in comparison with the rest of the Benguela system reflecting amplified SST changes. Decreasing SSTs accompanied increasing river discharge during times of increased precipitation in the WRZ, reflecting northerly shifted westerly winds during austral winter. We infer a control of past SST changes by processes not analogous to modern processes driving seasonal SST changes by changes through upwelling intensity. The findings suggest that late-Holocene SST changes in the southernmost Benguela upwelling system and the precipitation in the WRZ were both driven by latitudinal shifts of the austral westerly wind belt and associated changes in advection of cold sub-Antarctic waters and/or changes in Agulhas leakage of warm Indian Ocean waters.

Keywords

late Holocene, river runoff, sea-surface temperature, South Africa, winter rainfall zone

Introduction

South Africa is positioned between the warm western boundary Agulhas Current and the cool nutrient-rich eastern boundary Benguela Current and influenced by both tropical and temperate water masses and climate systems (Chase and Meadows, 2007; Chase et al., 2013; Shannon and Nelson, 1996; Tyson et al., 1996). Tropical systems bring summer rainfall to the northern and eastern parts of the summer rainfall zone (SRZ), where moisture from the Indian Ocean is the dominant source of precipitation (Chase and Meadows, 2007; Chase et al., 2015). In contrast, the winter rainfall zone (WRZ) (indicated in Figure 1), the smaller, southwestern section, is affected by temperate climatic influences. Precipitation here occurs as a result of seasonal northward shifts of the rain-bearing Southern Hemisphere Westerlies (SHW) over the southernmost tip of Africa (Stager et al., 2012; Tyson and Preston-Whyte, 2000). Climatic changes in the WRZ were suggested to be indicative of large-scale shifts in tropical and temperate climate zones (Carr et al., 2006; Chase and Meadows, 2007) with large shifts over glacial–interglacial timescales (Chase and Meadows, 2007; Chase and Thomas, 2007) and smaller shifts over millennial timescales (Hahn et al., 2015; Stager et al., 2012; Tyson et al., 2002).

At present, there is, however, a limited understanding of the climate dynamics in this region, particularly during the past ~2000 years, a time period that is relevant to future climate predictions (McGregor et al., 2015). A record of this time period would set an important benchmark for the region regarding its response to millennial and centennial climatic changes in the late Quaternary, including the major global climate phases such as the 'Little Ice Age' (LIA; 1350–1800 CE; Mann et al., 2002) and the Medieval Climate Anomaly (MCA; 950–1250 CE; Mann et al., 2009).

The linkage between the Benguela upwelling system (BUS; an oceanic system comprising the Benguela Current, its upwelling cells and filaments, the west coast mud belt, and the poleward undercurrent) and the continental rainfall in the Southern African

[1]Department of Oceanography, University of Cape Town, South Africa
[2]School of Geographic Sciences, East China Normal University, Shanghai, China
[3]MARUM–Center for Marine Environmental Sciences, University of Bremen, Germany
[4]Royal Netherlands Institute for Sea Research (NIOZ) and Utrecht University, Texel, The Netherlands
[5]Now at Institute for Geology, University of Hamburg, Germany

Corresponding author:
Robyn Granger, Department of Oceanography, University of Cape Town, University Avenue, Rondebosch 7701, Cape Town, South Africa.
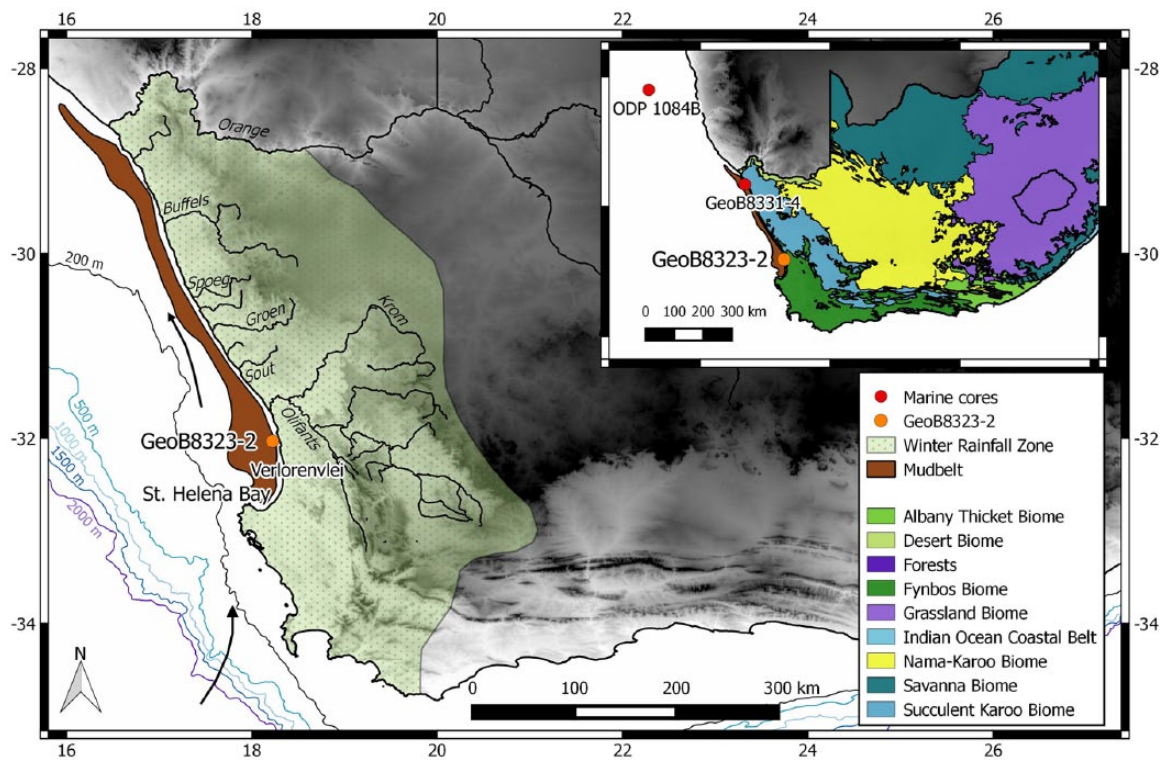Email: grnrob016@myuct.ac.za

Figure 1. Map of southwest Africa showing the extent of the winter rainfall zone (WRZ) and the rivers that drain the west coast of the country, including the Orange River and the Olifants River. GeoB8323-2 is located within the mud belt at 32°01.89 S, 18°13.19 E, while dots on the map insert represent other cores mentioned in the text. The core site is north of St Helena Bay and in close proximity to the estuarine lake Verlorenvlei. Bathymetric contours are 200, 500, 100, 1500, and 2000 m (sourced from GEBCO, www.gebco.com), and a transitional gradient of white to black is used to indicate terrestrial elevation (0–1500 m) (SRTM data v4, Jarvis et al. 2008). Biological data are sourced from Mucina and Rutherford (2006), and the WRZ is estimated using the WorldClim 1.4 data set (Hijmans et al., 2005).

WRZ during the late Holocene remains inadequately understood. To improve the understanding of the late-Holocene climate history of the WRZ and its relationship to oceanic changes, we investigated a marine sediment core which was recovered during the M57/1 *Meteor* cruise in January/February 2003 near St Helena Bay from 92-m water depth in the west coast mud belt (32°01.89 S, 18°13.19 E) (Herbert and Compton, 2007). The continuous record allows parallel reconstructions of oceanic and terrestrial climate changes for the past 2000 years (Herbert and Compton, 2007).

In order to assess how sea-surface temperatures (SSTs) in St Helena Bay have varied over the past 2 millennia as well as to investigate the nature and magnitude of hydrological change in the adjacent catchment basin, and the forcing mechanisms, we present here a new multi-proxy record (alkenone SST, grain size, and elemental concentrations) from the southernmost region of the BUS.

Modern climatology

Regional setting

The generally arid western half of southern Africa is traversed by several seasonal and perennial rivers. The largest of these, the Orange River, borders South Africa and Namibia and drains a substantial part of the SRZ (Meadows et al., 2002; Figure 1). All rivers within the 500-km coastal stretch between the Orange River and St Helena Bay (including the Olifants, Jakkals, and Langvlei Rivers) drain into the mud belt on the shelf of southwest Africa, making it an important depot of high-resolution sedimentary archives (Herbert and Compton, 2007). Close to St Helena Bay, the Olifants River discharges a large catchment extending into the WRZ. The fine terrestrial material derived from all rivers is transported southward along the inner shelf by a poleward-flowing undercurrent

(Herbert and Compton, 2007). Coarser sand and gravel grains discharged at the mouth of the Orange River follow the main path of the Benguela Current and move northward via the long-shore drift (Garzanti et al., 2014).

In contrast to the coast of Namibia, aeolian transport of dust is not a significant sediment source at this location. A study showing a latitudinal transect of terrestrial-derived material from the southwest African coast demonstrates that very little dust is blown to the Atlantic south of 20°S (Rommerskirchen et al., 2003). Furthermore, high-resolution satellite imagery from SeaWIFS (Sea-Viewing Wide Field-of-View Sensor) identifies almost no dust plumes occurring south of 28°S, that is, south of the Orange River mouth (Eckardt and Kuring, 2005). Other observational studies show that although southwest Africa currently contains vast sand surfaces with multiple pans, there is very little associated dust activity (Prospero et al., 2002; Vickery et al., 2013). Regarding the possible deposition of dust from sources further north, Gingele (1996) suggests that the prevailing wind directions in the south-east Atlantic (southerly and westerly) account for the lack of aeolian-deposited material in this region, inferring minor dust input over the past 4000 years. Therefore, aeolian transport is not considered to be a significant factor when determining the origin of mud belt sediments.

The WRZ

Onshore of the Benguela Current, a very steep north–south rainfall gradient along the western coast of South Africa promotes the existence of several biomes within the WRZ, namely, the Namib Desert, Succulent Karoo, and Fynbos Biomes (Mucina and Rutherford, 2006). This steep rainfall gradient is a contributing factor to the difficulty in establishing reliable, continuous paleo-environmental records from the region; rainfall patterns at

one location may not be representative of conditions further afield. Furthermore, high relief environments associated with high erosion rates and high rainfall seasonality may produce poor records, since erosion removes material for paleo-environmental reconstruction. Nevertheless, several Holocene paleo-environmental reconstructions have been successful in the regions of Verlorenvlei and the Cederberg Mountains, based on traditional wetland or lacustrine sedimentary proxies (e.g. Carr et al., 2015; Meadows and Baxter, 2001; Meadows et al., 1996; Stager et al., 2012). These studies have consistently identified low-amplitude vegetation changes in the WRZ during the Holocene. (Chase et al., 2015; Meadows et al., 2010; Quick et al., 2011; Valsecchi et al., 2013).

The WRZ is highly sensitive to hemispheric-scale climate changes and links with the SHW have been documented (Carr et al., 2015; Chase and Meadows, 2007; Chase et al., 2013; Stager et al., 2012; Weldeab et al., 2013). These studies suggest that equatorward shifts in SHW are coincident with rainfall increases in the WRZ, whereas southward migrations lead to drier conditions. Evidence of progressively freshwater conditions beginning at around 600 years before the present point toward increased SHW-derived precipitation (Carr et al., 2015; Cohen and Tyson, 1995; Stager et al., 2012) and are consistent with the findings of studies from further afield that a northward shift of SHW was experienced during this time (Lamy et al., 2001, 2002, 2010; Toggweiler et al., 2006).

The Benguela Current

Upwelling. A coastal upwelling system is one in which alongshore winds induce Ekman pumping of cold subsurface waters to the surface leading to enhanced primary productivity and lower SST (Stewart, 2009). The BUS, one of the world's major upwelling zones, follows the southwest African coast between 17 and 34°S. The BUS is unique among eastern boundary systems as both its northern and southern boundaries consist of warm water systems, namely, the Angola and the Agulhas Currents (Demarcq et al., 2003; Shillington, 1998). In the austral summer, when the South Atlantic anticyclone is farthest south, alongshore south-easterly winds induce near-shore upwelling accompanied by lower SSTs and higher primary productivity in this region (Hutchings et al., 2009; Shannon and Nelson, 1996). In contrast, during austral winter, cold front-associated winds dominate, suppressing upwelling and subsequently leading to higher SSTs and lower productivity (Lamont et al., 2015).

Additionally, large-scale seasonal climate differences in southwest Africa are likely related to dynamics in Antarctic frontal systems (Dixon et al., 2012; Sokolov and Rintoul, 2007). Variations in Antarctic sea ice respond to seasonal changes in insolation, leading to expansion of sea ice during winter and contraction during summer (Fischer and Jungclaus, 2011; Gildor and Tziperman, 2000). Cool winter conditions cause the oceanic fronts to migrate north creating strong SST gradients that intensify the SHW (Renssen et al., 2005; Sokolov and Rintoul, 2007). During cold periods with extensive sea ice, intensified onshore winds can bring increased moisture to southwestern Africa and suppress Benguela upwelling (Bard and Rickaby, 2009).

St Helena Bay. St Helena Bay, the southernmost part of the BUS, is a climatologically complex region because of its irregular coastline and relatively close proximity to influences emanating from the warm Agulhas Current (Figure 1). The bay is a distinctive feature along the southwest coast, located 80 km south of core site GeoB8323-2. The shape of the embayment, along with the West Coast Peninsula, promotes recirculation, which alters the natural equatorward flow of the Benguela Current (Pitcher and Nelson, 2006). Despite not being situated within one of the multiple intense upwelling cells, St Helena Bay still experiences upwelling offshore along the continental shelf, on which the mud belt is situated (Lamont et al., 2015). The region is influenced by the south-east trade winds in summer (DJF) and the westerly winds in winter (JJA), both of which act to influence local SSTs (Hutchings et al., 2012). Modern satellite-derived SSTs in St Helena Bay range from 14.3°C in summer to 15.6°C in winter with a mean annual SST of 14.9°C (Locarini et al., 2013). This small inter-annual and seasonal variability is characteristic of the bay (Hutchings et al., 2012).

Methods

Chronology

An age model for GeoB8323-2 was initially developed by Herbert and Compton (2007) and has recently been updated by Hahn et al. (2015) using a linear interpolation of six radiocarbon dates from bottom-dwelling gastropods and bivalves and a regional reservoir age offset of 146 ± 85 ^{14}C years (Dewar et al., 2012), together with the southern hemisphere marine calibration curve Marine13 (Reimer et al., 2013). Because of the paucity of foraminifera in mud belt sediments (Herbert and Compton, 2007), bivalves and gastropods were dated. More details on the age model can be found in Table 1 of this study and in Hahn et al. (2015).

GeoB8323-2 is 2.85 m in length, but results from both Herbert and Compton (2007) and Hahn et al. (2015) indicate the presence of a hiatus in the lower part of the core (below 227 cm). The sediment directly above the hiatus was initially dated to ~337 cal years before CE (Herbert and Compton, 2007). The sedimentation rate is consistently around 1 mm per year with the exception of the interval between 112 and 124 cm where the sedimentation rate almost doubles to ~1.8 mm per year. This sudden change may be because of uncertainty arising from closely spaced dated depth intervals (111 and 124 cm) and is not considered to be an accurate reflection of a change in deposition.

Core sub-sampling

For alkenone analysis of GeoB8323-2, 43 samples were taken with syringes, with an initial resolution of 5 cm (equivalent to an average sample resolution of 25 years) until 150 cm, below which a 10-cm resolution was used (ca. 100 years between samples). The upper part of the core was sampled at a higher resolution than the lower section. This was done to obtain a more detailed perspective of the recent past, particularly during the periods contemporaneous with the MCA (950–1250 CE) and 'LIA' (1300–1850 CE). Sample volumes ranged between 3 and 5 cm^3 of sediment, with dry sample weights between 2.5 and 6.5 g. All samples were freeze-dried and manually ground before analysis. For grain size determination, samples were air-dried prior to analysis. The uppermost 114 cm of the core was sampled for grain size at 1-cm intervals; thereafter it was sampled every 2 cm until 226 cm. Samples from below this depth were not included in this study because of the hiatus.

Alkenone analysis

Ground samples were extracted via accelerated solvent extraction in a DIONEX ASE200 at 100°C and 1000 psi. A solvent mixture of dichloromethane (DCM):methanol (MeOH) = 9:1 was used for extraction, running three cycles of 5 minutes each, whereafter lipid extracts were concentrated by rotary evaporation, followed by asphaltene precipitation via column separation using Na_2SO_4. Following saponification with 0.1 M KOH at 85°C for 2 hours to remove wax esters which potentially interfere with alkenone analysis, neutral fractions were separated by column chromatography

Table 1. AMS radiocarbon analyses of bulk TOC for GeoB8323-2, with additional dates from Herbert and Compton (2007).

Lab code	Core	Core depth (cm)	Material	14C age yr BP	Cal age yr BP (median probability)	+2σ	−2σ	Calibration data
Poz-67132	GeoB8323-2	0	bulk TOC	1035 ± 30 BP	461	519	391	Marine13.14c (Reimer et al., 2013)
Poz-67891	GeoB8323-2	12.5	gastropod	102.41 ± 0.98 pMC	'post-bomb'			
Poz-67130	GeoB8323-2	13	bulk TOC	960 ± 30 BP	409	476	357	Marine13.14c (Reimer et al., 2013)
Poz-67890	GeoB8323-2	39.5	gastropod	740 ± 70 BP	233	350	119	Marine13.14c (Reimer et al., 2013)
Poz-67128	GeoB8323-2	111	bulk TOC	2265 ± 30 BP	1726	1821	1643	Marine13.14c (Reimer et al., 2013)
Poz-64013	GeoB8323-2	111	gastropod	1700 ± 30 BP	1113	1168	1034	Marine13.14c (Reimer et al., 2013)
Poz-67129	GeoB8323-2	124	bulk TOC	2385 ± 30 BP	1868	1965	1774	Marine13.14c (Reimer et al., 2013)
Poz-63485	GeoB8323-2	176	bulk TOC	2835 ± 30 BP	2460	2559	2333	Marine13.14c (Reimer et al., 2013)
Poz-67131	GeoB8323-2	226	bulk TOC	3395 ± 35 BP	3119	3212	3012	Marine13.14c (Reimer et al., 2013)
Poz-63483	GeoB8323-2	252	bulk TOC	3580 ± 30 BP	3326	3414	3234	Marine13.14c (Reimer et al., 2013)
Poz-63484	GeoB8323-2	274	bulk TOC	5185 ± 35 BP	5400	5470	5314	Marine13.14c (Reimer et al., 2013)
Herbert and Compton (2007)								
104275	GeoB8323-2	124	gastropod	1790 ± 35 BP	1184	1266	1115	Marine13.14c (Reimer et al., 2013)
104273	GeoB8323-2	227	bivalve	2730 ± 35 BP	2287	2454	2184	Marine13.14c (Reimer et al., 2013)
GrA-24895	GeoB8323-2	285	gastropod	11,420 ± 35 BP	12,726	12,862	12,585	Marine13.14c (Reimer et al., 2013)

Ages were calibrated using OXCAL software (Bronk Ramsey, 2001) and the Marine13.14c model (Reimer et al., 2013). An additional reservoir age of 146 ± 14C years (Dewar et al., 2012) was used.

using 1% deactivated silica and hexane to remove a hydrocarbon fraction and DCM to isolate a ketone fraction.

Alkenone unsaturation ratios were determined by gas chromatography/flame ionization detection (GC-FID) using a Thermo Fisher Scientific Focus GC-FID at MARUM, University of Bremen. The GC-FID was equipped with a split/splitless injector and a 60-m DB-5ms column. Analyses of an external alkane standard of known concentrations were performed repeatedly. Precision of compound quantifications based on replicate standard measurements (1σ) is 5%. The $U^{K'}_{37}$ method, based on the di- and tri-unsaturated C_{37} alkenones, is described by Prahl and Wakeham (1987). $U^{K'}_{37}$ is calculated using the following ratio:

$$U^{K'}_{37} = \frac{C37:2}{\left(C37:2 + C37:3\right)}$$

The index is converted to SST using the calibration by Müller et al. (1998):

$$SST = \frac{U^{K'}_{37} + 0.044}{0.033}$$

All samples were measured in duplicate, in accordance with standard operating procedure, yielding an absolute $U^{K'}_{37}$ error of $0.010 \, U^{K'}_{37}$ units translating to a mean analytical error in SST estimation of 0.09°C. The calibration error is taken as 1.0°C (Müller et al., 1998).

Particle-size and end-member analysis

Grain size analysis was performed using a Malvern® Mastersizer 2000, which resulted in 78 size classes, from 0.28 to 2000 μm. Prior to measurement, bidest water was added to the samples and thoroughly mixed to ensure complete particle separation. Samples were then filtered through a 5-mm sieve. An obscuration level of between 10% and 20% was used for all samples, with background levels being measured before each run. Grain size measurements were conducted in duplicate for each sample.

An end-member modeling algorithm (Stuut et al., 2004) was applied to the results of the grain size analysis in order to determine changes in relative proportions of characteristic size spectra (Weltje, 1997). The total variability accounted for by each of the end-member models is represented by r^2_{mean}, and this factor is used to determine the optimal number of end members. A three end-member model was chosen for this study, where $r^2_{mean} = 0.70$ (70% of variability is accounted for).

X-ray fluorescence scanning

X-ray fluorescence (XRF) core scanning was performed on GeoB8323-2 in 2-cm increments by an Avaatech XRF Scanner at MARUM (University of Bremen), with a counting time of 30 s. Excitation potential and current were fixed at 10 kV and 250 μA, respectively. A more detailed description of XRF scanning methods can be found in the work by Hahn et al. (2015). The confounding effects of variations in of grain size and water content on XRF scanning data can be eliminated using elemental ratios (Jansen et al., 1998; Kido et al., 2006). This study focuses on the Fe/K ratio as an indicator of climate-induced variations in chemical weathering. Since K is more easily leached from soils than less mobile elements, such as Fe, soils formed during more humid conditions have higher Fe/K ratios (Govin et al., 2012).

Results

SSTs

The oldest part of the GeoB 8323-2 record reveals an initial decrease in SST from around 250 BCE to 250 CE, before increasing during the following 200 years (Figure 2a). Significant variability occurred from this point onward, and maximum SST (16.6°C) was recorded at 900 CE. Subsequent to this peak, a rapid decline occurred until about 1600 CE. This was followed by a 300-year colder-than-average period in the southern Benguela, although variability remained high, and a distinctive warming trend was present during this time.

The record reveals a long-term decline in SST over the past 2000 years (Figure 2a). This trend becomes more pronounced at around 700 CE, lasting until about 1700 CE, during which time the rate of cooling increased. Examination at shorter timescales reveals high amplitude variability (compared with Figure 2b and c) overlaying the long-term cooling trend, with a temperature range of 5.6°C (Figure 2a).
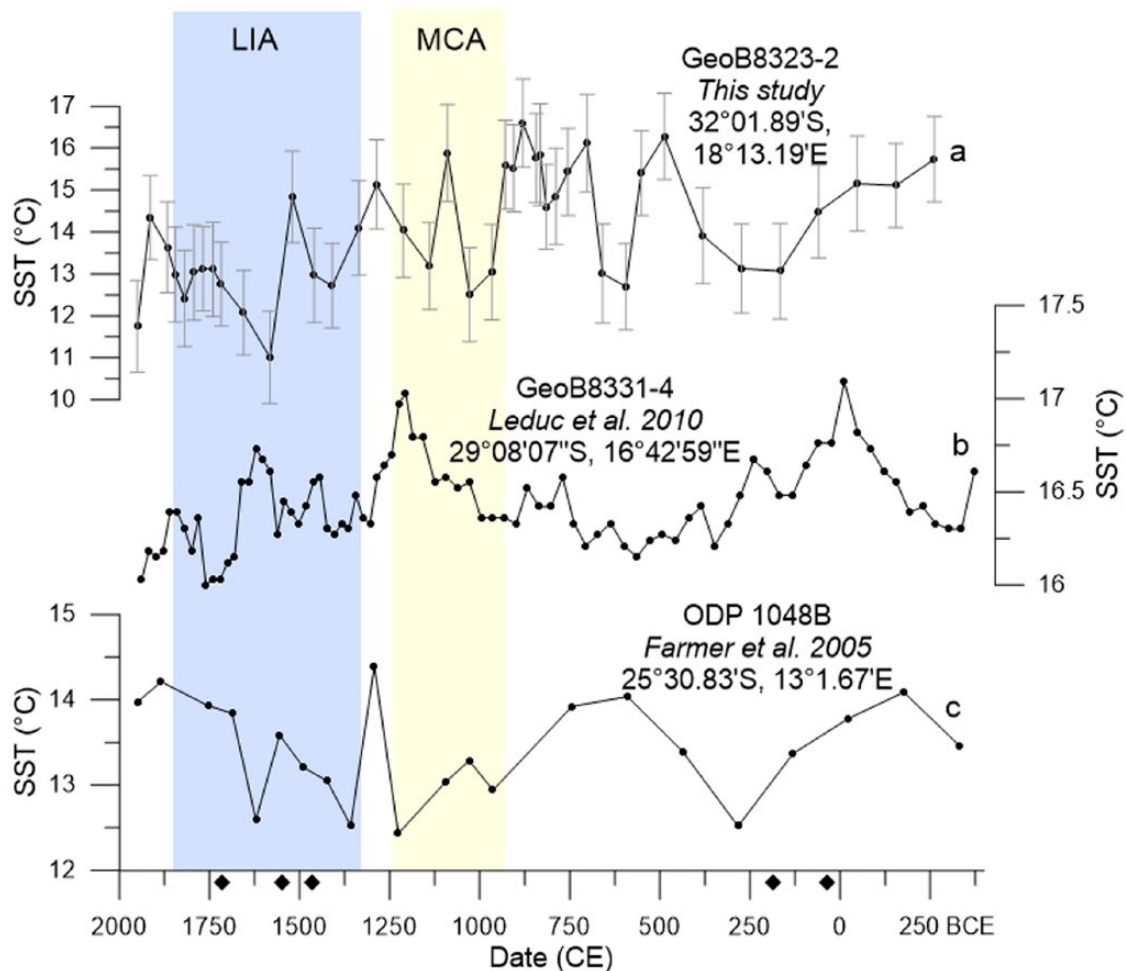
Figure 2. Benguela alkenone-derived sea-surface temperature (SST) variations as reconstructed from (a) GeoB8323-2 (this study), (b) GeoB8331-4 (Leduc et al., 2010), and Mg/Ca-derived SST reconstructed from (c) (Farmer et al., 2005; ODP 1084B). Mean values of GeoB8323-2 obtained from duplicate runs are plotted, with error bars representing absolute deviations between the duplicate analyses (<0.21C°) added to the calibration error (1°C). Black diamonds indicate age control measurements. The 'Little Ice Age' and Medieval Climate Anomaly are represented by shaded rectangles.

Grain size

Figure 3a shows the resulting ratios of the three end-member model, with Figure 3b displaying the eigenvalues and their corresponding end-member number. Grain size analysis of core GeoB8323-2 reveals a unimodal distribution in the particle size distributions (Figure 3c). Figure 3a shows the resulting ratios of the three end-member model. The three members (EM1, EM2, and EM3) have three clearly defined modal sizes at 19, 12, and 8 μm, respectively.

Fine-grained sediment (EM3) dominated deposition prior to 800 CE, representing more than 43% at any given time. A stable period of deposition characterized only by low-amplitude changes in grain size proportions occurred from about 250 to 800 CE, during which the largest percentage of the material is EM3. The coarse fraction, EM1, is only present in very small quantities prior to 800 CE and is absent from ca. 400 to 800 CE.

At around 800 CE, a rapid shift to coarser material (EM1 and EM2) occurred, followed by higher variability in coarse and fine fractions over the subsequent 800 years (Figure 3a). A second large increase in EM1 occurred at around 1600 CE, after which fine fractions again dominate the sediments, reaching up to 78% of total grains. Following this second increase, the coarse grain size fraction becomes increasingly dominant during the next 200 years. During this time, the portion of medium-sized grains decreases until it reaches zero at around 1850 CE. Figure 3a shows that a maximum in coarse grain size (EM1) is centered at

about 1800 CE, after which a decrease in EM1 and an increase in EM3 are observed.

Fe/K elemental ratio

The lowest values for the Fe/K ratio are found prior to 600 CE, a period in which Fe/K is relatively stable (Figure 4a). After this, the ratio increases until about 1250 CE, at which point an interval of lower values, lasting for approximately 150 years, is detected. Fe/K increases again from around 1550 CE. The final 350 years (i.e. from 1600 CE onward) witness the highest values observed in the record, with very high values occurring at around 1900 CE before a sharp drop occurs toward the present.

Discussion

Modern SST in St Helena Bay

Comparison of core-top alkenone-derived SST from GeoB8323-2 with satellite-derived mean annual SSTs (14.9°C, Locarini et al., 2013) reveals similar temperatures, with the most recent data point (ca. 1900 CE) reflecting a temperature estimate of 14.4°C. The discrepancy between the two SST estimates is within the $U^{K'}_{37}$ SST calibration error of 1°C (Müller et al., 1998). Therefore, reconstructed SST values are assumed to reflect mean annual values. In order to identify the links between SST changes and terrestrial hydrology in the area of the southernmost BUS,
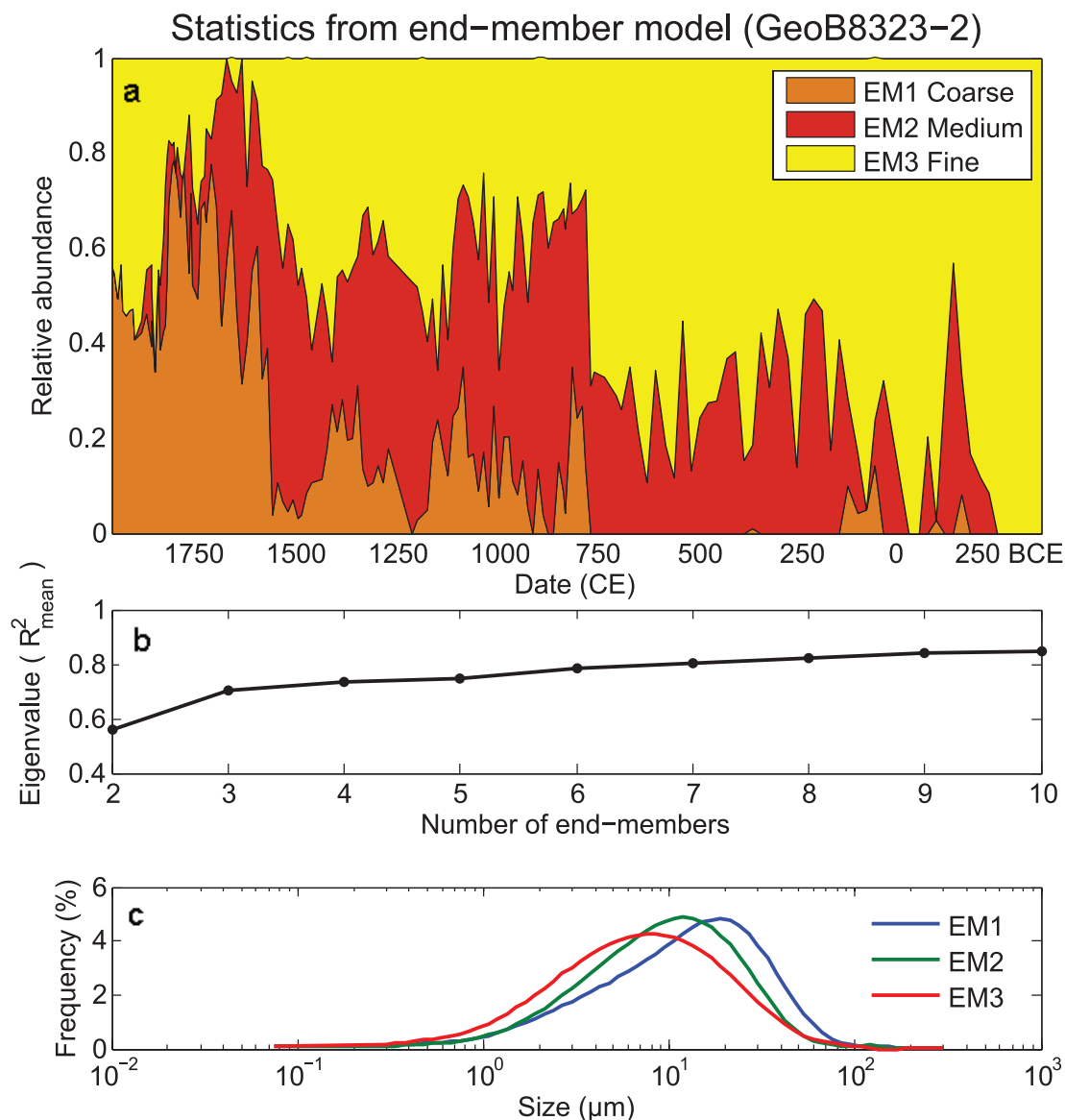
Figure 3. Results generated from end-member modeling. (a) Temporal changes in ratio proportions using a three end-member model. Plot shows relative abundances of EM1 (coarse) to EM3 (fine). (b) Fraction of variation explained by the amount of end members. (c) Unimodal frequency curves of grain size classes, using a three end-member model.

we first discuss the changes in precipitation in the WRZ and their controls and will later connect these inferences with the SST development.

Late-Holocene terrestrial changes in hydrology

Source of material. EM1, the coarse grain size fraction, exhibited sharp changes during the past two millennia (Figure 3a). Shifts toward a greater proportion of the coarse end member occurred at 800 and 1600 CE. The Fe/K elemental record corresponds to the EM variations, with sharp changes in both records occurring at similar times (Figure 4). The Fe/K ratio indicates an increase in chemical weathering associated with higher humidity (Govin et al., 2012). Whereas K is easily leached from soils under humid conditions, Fe is not as readily mobilized from the soil and thus becomes enriched (Govin et al., 2012). The general resemblance between both records suggests that chemical weathering and input of larger grain sizes were driven by the same process.

While the majority of the mud belt sediments is provided by the Orange River, it will not provide the coarse end member as the poleward undercurrent lacks sufficient energy to keep coarser grain sizes in suspension (Garzanti et al., 2014; Shannon and

Nelson, 1996). Other studies have indicated the overprint of Orange River derived material in the mud belt by local-derived pollen (Zhao et al., 2016), plant organic material (Herrmann et al., 2016, 2017), and inorganic sediments (Hahn et al., 2015). The latter showed that Nd and Sr isotope ratios at site GeoB8323-2 do not correspond to those offshore of the Orange River and instead are representative of the Olifants River catchment. Therefore, the Orange River likely is not the primary source of the increasing proportion of coarse grain size (EM1) in GeoB8323-2 (Figure 4c). In principle, the grain size changes in sediments can be influenced by many processes, such as sea-level changes (Rogers and Rau, 2006), microfossil abundance, winnowing by bottom currents (Henderson, 2002; Prins et al., 2002), as well as changes in terrestrial input. Sea-level variations during the past 2000 years varied approximately ±1 m (Compton, 2001) and are thus unlikely to have affected the record. Additionally, mud belt sediments are generally poor in foraminifera, not providing sufficient material for dating (Herbert and Compton, 2007), suggesting that variable microfossil abundance is not the primary control. The broad resemblence of increasing grain size (Figure 4c) with increasing chemical weathering (Fe/K ratios; Figure 4a) and the correspondence of increasing grain sizes with higher occurrence of dilute
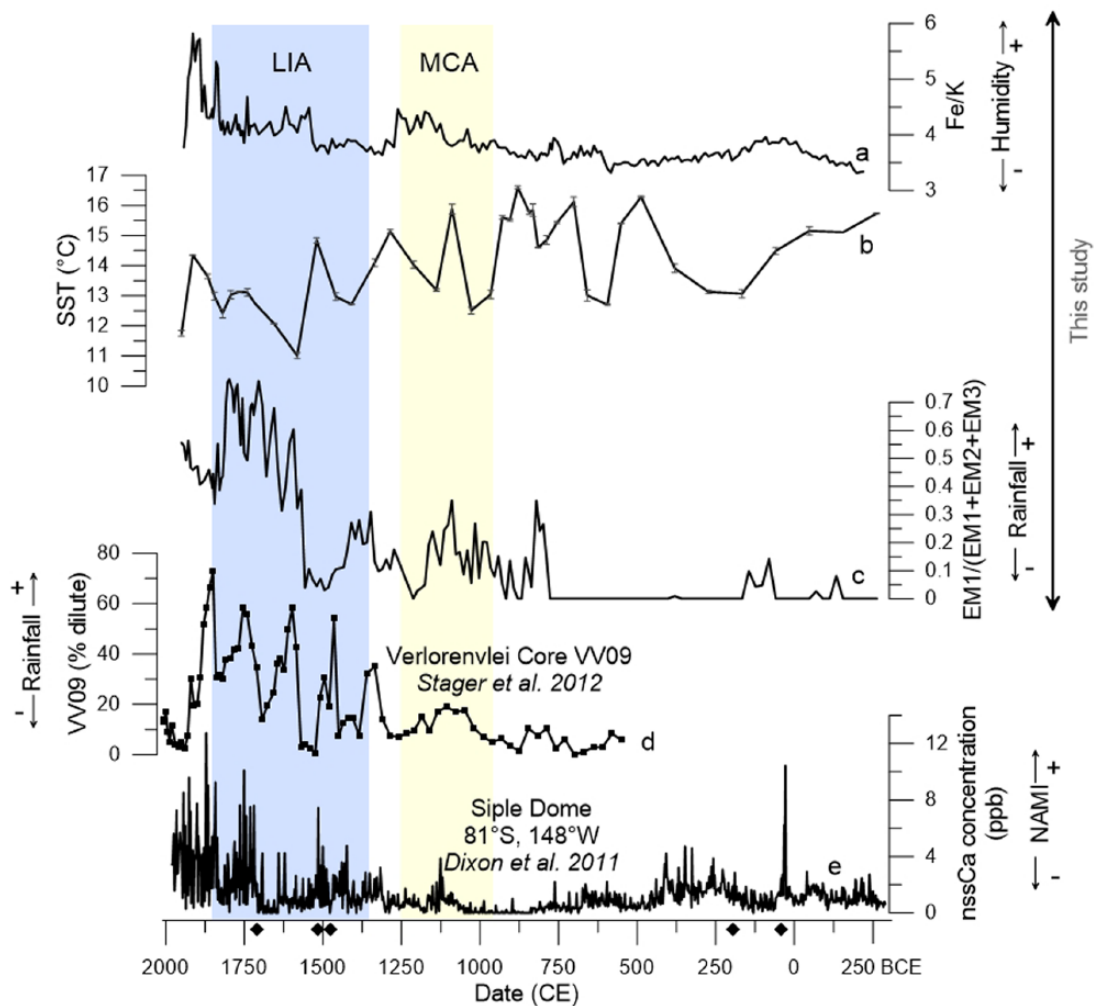
Figure 4. (a) GeoB8323-2 Fe/K ratio as a proxy for chemical weathering; (b) GeoB8323-2 Benguela Current SST in St Helena Bay; (c) GeoB8323-2 1EM3 coarse grain size (higher rainfall) variation; (d) diatom concentration showing the percentage of dilute-water diatoms, indicating freshwater input into lake Verlorenvlei and serving as a proxy for precipitation in the lake catchment (Stager et al., 2012); and (e) variation in nss-Ca from Siple Dome, indicative of NAMI fluctuations (Dixon et al., 2012). Black diamonds indicate age control measurements, and the 'Little Ice Age' and Medieval Climate Anomaly are indicated by the shaded rectangles.

diatoms (indicating higher lake levels) in nearby lake Verlorenvlei (Stager et al., 2012; Figure 4d) suggests that indeed variable terrestrial runoff of coarse sedimentary material is the cause of grain size variations at this location and not winnowing by bottom currents. As WRZ precipitation in the Olifants River catchment is derived from the westerlies in austral winter, an additional effect of winnowing by increased storminess cannot be ruled out but would be indicative of the same process, that is, a more northerly position of the westerlies bringing more precipitation to the WRZ. Changes in the relative abundance of coarse grain sizes are thus interpreted as being cause by changing local terrestrial hydrology, that is, higher rainfall in the WRZ associated with an increase in local river transport and possibly sorting of bottom sediments by increased storminess. A long-term increase in Olifants River discharge because of increasing wetter conditions is most likely the underlying cause for the observed grain size and elemental changes supporting the interpretation proposed by Hahn et al. (2015) in their analysis of the WRZ.

Climatic evolution. During the period between 250 BCE until about 750 CE, variations in terrestrial hydrology (Figure 4a and c) depict a relatively stable dry climate in the southwest river catchment regions within the WRZ, as compared with the latest Holocene. Within this interval, driest conditions were observed between 250 and 0 BCE. A dry WRZ during this time coincides

with the findings of Carr et al. (2015) documenting relatively arid conditions from 550 BCE to 1000 CE. After this period, the SHW started to shift to a more northerly position, and humidity and rainfall in the WRZ increased markedly within half a century. The grain size and elemental records, through the introduction of coarse fluvial material from the Olifants River, show that the period from 800 to 1600 CE was wetter but highly variable, fluctuating between wet and dry conditions.

According to our records, a shift toward more consistently wetter conditions occurred at about 1600 CE, probably forced by a northward migration of the SHW. Grain size data indicate that wet conditions were prevalent for the next 350 years. The Fe/K ratio reflects a sharp increase in humidity at the same time. This increase in moisture availability in the WRZ during the past several hundred years is in accordance with several studies which have documented a rapid late-Holocene shift toward wetter conditions in the WRZ (Carr et al., 2015; Stager et al., 2012), although data from GeoB8323-2 show this to have occurred roughly 200 years after the changes documented in the aforementioned studies. This discrepancy is most likely a result of uncertainties in age models of both terrestrial and marine archives.

Limited ages are recorded for GeoB8323-2 post-1900 (Hahn et al., 2015), and changes subsequent to this time are addressed with caution. However, a noticeable decrease in WRZ rainfall is apparent from 1800 to 1900 CE, as shown by grain size data.

Studies from nearby lake Verlorenvlei have previously documented intensification in aridity after wet conditions peaked at around 1850 CE (Figure 4d; Carr et al., 2015; Stager et al., 2012). This most recent change is interpreted as a southward shift in the SHW supported by the aforementioned studies. However, it is important to note the potential anthropogenic influences that may have affected the signal during the past 200–300 years, since environmental impacts became more prominent in the years following colonial occupation and associated agricultural practices (Baxter and Meadows, 1999; Hahn et al., 2015; Stager et al., 2012).

SST control during the late Holocene

A comparison between the SST record at site GeoB8323-2 and records further north in the BUS (Farmer et al., 2005; Leduc et al., 2010; Figure 2) shows that the SST range (~5.6°C) for GeoB8323-2 is larger than those recorded at the northern BUS sites (Farmer et al., 2005; Leduc et al., 2010) as well as being much larger than the modern seasonal SST range in the southern region (Hutchings et al., 2012). These two observations suggest that SSTs in the St Helena Bay region during the Holocene were (1) controlled by different processes than those directly affecting sites further north in the BUS and (2) amplified relative to a sole upwelling control.

In the modern BUS, SST changes due to changes in upwelling are primarily driven by changes in south-easterly, that is, local, trade winds inducing Ekman pumping (Nelson and Hutchings, 1983). In contrast to the northern sites which experience perennial upwelling, upwelling in the southernmost BUS occurs only during austral summer when the South Atlantic high-pressure cell is located furthest south. The long-term cooling at site GeoB8323-2 could thus be because of an increase in upwelling during austral summer driven by stronger south-east trade winds or a shift from seasonal to perennial upwelling in St Helena Bay. Intensified upwelling during austral summer at site GeoB8323-2 would require intensified trade winds leading to stronger Ekman pumping. We do not see a similar upwelling increase (SST lowering) at the site off the Orange River (GeoB8331-4) which speaks against intensified south-east summer trades as a cause for the SST decrease in GeoB8323-2. Additionally, reconstructed summer SSTs from a site at 50°S south of Cape Town (Nielsen et al., 2004) show a warming in the Atlantic sector of the Southern Ocean over the past 4000 years. This speaks against an increased zonal pressure gradient during austral summer which would induce stronger south-east trades. Intensified summer upwelling is thus not likely to be the cause for the cooling at site GeoB8323-2. A switch from seasonal to perennial upwelling in the southernmost BUS would require a southern shift of the SHW during austral winter, which otherwise prohibits upwelling at site GeoB8323-2 because of onshore winds. As discussed above (in section 'Late-Holocene terrestrial changes in hydrology'), the late Holocene in the WRZ is characterized by strong precipitation increases, exactly at times when significant SST decreases occurred. As inferred, these precipitation increases were likely caused by a northward shift in the position of the SHW during austral winter. As in this scenario, onshore winds are preventing coastal upwelling, this process rules out a shift from seasonal to perennial upwelling at site GeoB8323-2. Changes in upwelling intensity and a switch from seasonal to perennial upwelling activity at site GeoB8323-2 therefore do not explain the observed SST variability over the late Holocene in the southernmost Benguela. Processes controlling the SST variability in the southernmost Benguela are thus non-analogous to modern seasonal SST-controlling processes. To identify these, we must invoke other processes potentially affecting SSTs in this area.

The first possible explanation is enhanced advection of cold sub-Antarctic waters from the South Atlantic Gyre (Farmer et al., 2005) into the Benguela system when the SHW are located furthest north. A second potential control is via variable leakage of warm Indian Ocean Agulhas waters entering the southern BUS by warm water 'ring shedding' at the Agulhas retroflection (de Ruijter et al., 1999; Garzoli et al., 1999; Schouten et al., 2000). Although the southernmost near-coastal Benguela is not located under the direct pathway of Agulhas rings entering the Atlantic Ocean (Olson and Evans, 1986), warm Indian Ocean waters can influence the properties of the Southern Benguela. Strong exchange between surrounding waters and Agulhas rings means that the latter has the potential to alter SSTs even outside the direct ring trajectory (Boebel et al., 2003; Richardson et al., 2003; Schmid et al., 2003). Therefore, variable Agulhas leakage of warm Indian Ocean waters presents a second possible mechanism to affect SST in the southernmost Benguela.

The amount of warm water entrained into the BUS is hypothesized to be regulated by changes in the position of the SHW, but there is debate over exactly how this mechanism operates. The accepted model suggests the increase (decrease) in Agulhas leakage with a southward (northward) migration of the SHW, through a 'valve' mechanism. A northerly position of the SHW limits the amount of warm water flow from the Agulhas to the BUS, since in this position the wind belt effectively blocks westward-moving rings (Bard and Rickaby, 2009; Biastoch et al., 2009; Zahn et al., 2010). Via the same understanding, southward shifts in the SHW would allow for increased frequency of warm water incursions, thereby increasing SST in the southernmost Benguela.

Based on model experiments, Durgadoo et al. (2013) recently proposed an alternative mechanism controlling Agulhas leakage throughflow, where the volume is determined by the redistribution of momentum input by winds. This model associates increased (decreased) leakage with an equatorward (poleward) in wind intensity and contrasts with the 'valve' mechanism. This contradiction can be resolved by examining the position and intensity of the SHW at a modern-day intra-annual timescale. During winter months, although located further north, the core intensity of the SHW is weaker than during summer. Therefore, a more intense wind belt may indicate a higher latitude SHW (Biastoch et al., 2009; Durgadoo et al., 2013). Although the focus of our study is not to determine the controls of Agulhas leakage, our data (decreasing SST associated with a northward shift of the SHW) speak against an increased flow of warm Agulhas waters into the South Atlantic Ocean with northward shifted SHW and favor the classical 'valve' model.

In summary, latitudinal changes in the SHW thus control both continental rainfall in the WRZ and SSTs in the southernmost BUS. At previously published Benguela sites, GeoB8331-4 and ODP 1084B, the SHW and Agulhas leakage are geographically too far away to impact the system; however, these two elements appear to be highly influential at the southerly position of GeoB8323-2, making this location ideal for observing connected SHW-related SST and precipitation changes. From ~250 BCE to ~250 CE, a noticeable decline in SST at GeoB8323-2 (Figure 4b) occurred parallel to decreasing SSTs at locations further north in the BUS (Figure 2, Farmer et al., 2005; Leduc et al., 2010) which is not associated with a precipitation increase in the WRZ (Figure 4; Hahn et al., 2015; Stager et al., 2012). This SST decrease thus deviates from the concept of an SST control by cold water advection and/or decreased Agulhas leakage. Local-scale upwelling by increased south-easterly winds may have contributed to this SST decline at times when the SHW were located far south. From this, we suggest that when the SHW were far south and less proximal to the Agulhas and the Benguela Current regions, local scale forcing of SST became important in the St Helena Bay region making its SST signal similar to locations further north in the system.

During the last millennium, our data suggest a progressively equatorward movement of the SHW, with the most northerly

position having occurred between 1600 and 1900 CE (lowest SST). This finding correlates well with the increase in non-sea salt Calcium (nss-Ca) in the Antarctic Siple Dome ice core record (Dixon et al., 2012). This connection, outlined more fully in the work by Stager et al. (2012), suggests a northward expanded SHW belt transporting more dust to Antarctica (Dixon et al., 2012; Stager et al., 2012). The record indicates an increase over the past 700 years (Figure 4e), consistent with the inferred northward shift in the SHW by our data and the data by Stager et al. (2012). In addition to correlating with West Antarctica, our data fit to findings from the Peru-Chile upwelling system (Lamy et al., 2010) documenting the large-scale connections of SHW-driven changes around Antarctica.

Conclusion

This study presents the first SST record for the southernmost BUS covering the past 2000 years and investigates the linkages between oceanic and terrestrial climate changes at the southernmost tip of Africa during the late Holocene.

Geochemical and grain size data suggest increasing precipitation in South Africa's WRZ in the late Holocene, inferred to be driven by northward migration of the SHW in accordance with previous studies. The increasing precipitation in the WRZ was associated with a long-term cooling over the past 2000 years. The relatively large SST variations at this location were found to have had no relationship to upwelling-driven SST changes further north in the BUS except in times of southernmost positioning of the SHW, prior to 800 BCE. In contrast to modern seasonal SST variations driven by austral summer upwelling, we infer that SSTs in the southern BUS were influenced by amplifying processes such as variable advection of cold sub-Antarctic waters and/or influences of warm Agulhas waters when the SHW were located further north than under present-day conditions. In summary, SST changes during the past 2000 years in this area were not primarily upwelling induced but instead driven by large-scale forcing of latitudinal migrations in the SHW. Northerly-positioned SHW reduced Agulhas warm water leakage and re-directed colder waters into the BUS. When the SHW were located further south, large-scale atmospheric features became less important, and SST was governed chiefly by local winds driving upwelling. In conjunction, these processes led to amplified SST changes in the southern BUS relative to the remainder of the system making it sensitive to large-scale oceanic and atmospheric controls.

References

Bard E and Rickaby REM (2009) Migration of the subtropical front as a modulator of glacial climate. *Nature* 460(7253): 380–383.

Baxter AJ and Meadows ME (1999) Evidence for Holocene sea level change at Verlorenvlei, Western Cape, South Africa. *Quaternary International* 56: 65–79.

Biastoch A, Boening CW, Schwarzkopf FU et al. (2009) Increase in Agulhas leakage due to poleward shift of Southern Hemisphere westerlies. *Nature* 462: 495–499.

Boebel O, Rossby T, Lutjeharms J et al. (2003) Path and variability of the Agulhas Return Current. *Deep Sea Research Part II* 50: 35–56.

Bronk Ramsey C (2011) Development of the radiocarbon calibration program OxCal. *Radiocarbon* 43: 355–363.

Carr AS, Boom A, Chase BM et al. (2015) Holocene sea level and environmental change on the west coast of South Africa: Evidence from plant biomarkers, stable isotopes and pollen. *Journal of Paleolimnology* 53: 415–432.

Carr AS, Thomas DSG, Bateman MD et al. (2006) Late Quaternary palaeoenvironments of the winter-rainfall zone of southern Africa: Palynological and sedimentological evidence from the Agulhas Plain. *Palaeogeography, Palaeoclimatology, Palaeoecology* 239(1–2): 147–165.

Chase BM and Meadows ME (2007) Late Quaternary dynamics of southern Africa's winter rainfall zone. *Earth-Science Reviews* 84(3–4): 103–138.

Chase BM and Thomas DSG (2007) Multiphase late Quaternary aeolian sediment accumulation in western South Africa: Timing and relationship to palaeoclimatic changes inferred from the marine record. *Quaternary International* 166(1): 29–41.

Chase BM, Boom A, Carr AS et al. (2013) Holocene climate change in southernmost South Africa: Rock hyrax middens record shifts in the southern westerlies. *Quaternary Science Reviews* 82: 199–205.

Chase BM, Lim S, Chevalier M et al. (2015) Influence of tropical easterlies in southern Africa's winter rainfall zone during the Holocene. *Quaternary Science Reviews* 107: 138–148.

Cohen AL and Tyson PD (1995) Sea surface temperature fluctuations during the Holocene off the south coast of Africa: Implications for terrestrial climate and rainfall. *The Holocene* 5(3): 304–312.

Compton J (2001) Holocene sea-level fluctuations inferred from the evolution of depositional environments of the southern Langebaan Lagoon salt marsh, South Africa. *The Holocene* 11(4): 395–405.

de Ruijter WPM, Biastoch A, Drijfhout SS et al. (1999) Indian-Atlantic interocean exchange: Dynamics, estimation and impact. *Journal of Geophysical Research* 104(C9): 20885–20910.

Demarcq H, Barlow RG and Shillington FA (2003) Climatology and variability of sea surface temperature and surface chlorophyll in the Benguela and Agulhas ecosystems as observed by satellite imagery. *African Journal of Marine Science* 25(1): 363–372.

Dewar G, Reimer PJ, Sealy J et al. (2012) Late-Holocene marine radiocarbon reservoir correction (ΔR) for the west coast of South Africa. *The Holocene* 22(12): 1481–1489.

Dixon DA, Mayewski PA, Goodwin ID et al. (2012) An ice-core proxy for northerly air mass incursions into West Antarctica. *International Journal of Climatology* 32: 1455–1465.

Durgadoo J, Loveday B, Reason C et al. (2013) Agulhas leakage predominantly responds to the southern hemisphere westerlies. *Journal of Physical Oceanography* 43: 2113–2131.

Eckardt FD and Kuring N (2005) SeaWiFS identifies dust sources in the Namib Desert. *International Journal of Remote Sensing* 26(19): 4159–4167.

Farmer EC, deMenocal PB and Marchitto TM (2005) Holocene and deglacial ocean temperature variability in the Benguela upwelling region: Implications for low-latitude atmospheric circulation. *Paleoceanography* 20(2): 1–16.

Fischer N and Jungclaus JH (2011) Evolution of the seasonal temperature cycle in a transient Holocene simulation: Orbital forcing and sea-ice. *Climate of the past* 7: 1139–1148.

Garzanti E, Vermeesch P, Andò S et al. (2014) Ultra-long distance littoral transport of Orange sand and provenance of the Skeleton Coast Erg (Namibia). *Marine Geology* 357: 25–36.

Garzoli SL, Richardson PL, Rae CMD et al. (1999) Three Agulhas Rings observed during the Benguela Current experiment. *Journal of Geophysical Research* 104: 20971–20985.

Gildor H and Tziperman E (2000) Sea ice as the glacial cycle's climate switch: Role of seasonal and orbital forcing. *Paleoceanography* 15(6): 605–615.

Gingele FX (1996) Holocene climatic optimum in southwest Africa – Evidence from the marine clay mineral record. *Palaeogeography, Palaeoclimatology, Palaeoecology* 122: 77–87.

Govin A, Holzwarth U, Heslop D et al. (2012) Distribution of major elements in Atlantic surface sediments (36°N-49°S): Imprint of terrigenous input and continental weathering. *Geochemistry, Geophysics, Geosystems* 13(1): 1–23.

Hahn A, Compton J, Meyer-Jacob C et al. (2015.) Holocene paleo-climatic record from the South African Namaqualand mudbelt: A source to sink approach. *Quaternary International* 404: 121–135.

Henderson GM (2002) New oceanic proxies for paleoclimate. *Earth and Planetary Science Letters* 203: 1–13.

Herbert CT and Compton J (2007) Geochronology of Holocene sediments on the western margin of South Africa. *South African Journal of Geology* 110(2–3): 327–338.

Herrmann N, Boom A, Carr AS et al. (2016) Sources, transport and deposition of terrestrial organic material: A case study from southwestern Africa. *Quaternary Science Reviews* 149: 215–229.

Herrmann N, Boom A, Carr AS et al. (2017) Hydrogen isotope fractionation of leaf wax n-alkanes in southern African soils. *Organic Geochemistry* 109: 1–13.

Hijmans RJ, Cameron SE, Parra JL et al. (2005) Very high resolution interpolated climate surfaces for global land areas. *International Journal of Climatology* 25: 1965–1978.

Hutchings L, Jarre A, Lamont T et al. (2012) St Helena Bay (southern Benguela) then and now: Muted climate signals, large human impact. *African Journal of Marine Science* 34(4): 559–583.

Hutchings L, van der Lingen CD, Shannon LJ et al. (2009) The Benguela current: An ecosystem of four components. *Progress in Oceanography* 83(1–4): 15–32.

Jansen JH, Van Der Gaast SJ, Koster B et al. (1998) CORTEX, a shipboard XRF-scanner for element analyses in split sediment cores. *Marine Geology* 151(1–4): 143–153.

Jarvis A, Reuter HI, Nelson A et al. (2008) Hole-filled SRTM for the globe Version 4. Available at: http://srtm.csi.cgiar.org.

Kido Y, Koshikawa T and Tada R (2006) Rapid and quantitative major element analysis method for wet fine-grained sediments using an XRF microscanner. *Marine Geology* 229(3–4): 209–225.

Lamont T, Hutchings L, van den Berg M et al. (2015) Hydrographic variability in the St. Helena Bay region of the southern Benguela ecosystem. *Journal of Geophysical Research: Oceans* 120: 2920–2944.

Lamy F, Hebbeln D, Röhl U et al. (2001) Holocene rainfall variability in southern Chile: A marine record of latitudinal shifts of the Southern Westerlies. *Earth and Planetary Science Letters* 185: 369–382.

Lamy F, Kilian R, Arz HW et al. (2010) Holocene changes in the position and intensity of the southern westerly wind belt. *Nature Geoscience* 3(10): 695–699.

Lamy F, Rühlemann C, Hebbeln D et al. (2002) High- and low-latitude climate control on the position of the southern Peru-Chile Current during the Holocene. *Paleoceanography* 17(2): 16-1–16-10.

Leduc G, Herbert CT, Blanz T et al. (2010) Contrasting evolution of sea surface temperature in the Benguela upwelling system under natural and anthropogenic climate forcings. *Geophysical Research Letters* 37(20): 1–5.

Locarini RA, Mishonov AV, Antonov JI et al. (2013) *World Ocean Atlas 2013, Volume 1: Temperature* (NOAA Atlas NESDIS 73). Silver Spring, MD: NOAA, pp. 40.

McGregor HV, Evans MN, Goosse H et al. (2015) Robust global ocean cooling trend for the pre-industrial Common Era. *Nature Geoscience* 8: 671–678.

Mann ME, MacCracken MC, Perry JS et al. (2002) Little Ice Age. *Encyclopedia for Global Environmental Change* 1: 504–509.

Mann ME, Zhang Z, Rutherford S et al. (2009) Global signatures and dynamical origins of the Little Ice Age and Medieval Climate Anomaly. *Science* 326: 1256–1260.

Meadows ME and Baxter AJ (2001) Holocene vegetation history and palaeoenvironments at Klaarfontein Springs, Western Cape, South Africa. *The Holocene* 11(6): 699–706.

Meadows ME, Baxter AJ and Parkington J (1996) Late Holocene environments at Verlorenvlei, Western Cape Province, South Africa. *Quaternary International* 33: 81–95.

Meadows ME, Chase BM and Seliane M (2010) Holocene palaeoenvironments of the Cederberg and Swartruggens mountains, Western Cape, South Africa: Pollen and stable isotope evidence from hyrax dung middens. *Journal of Arid Environments* 74(7): 786–793.

Meadows ME, Rogers J, Lee-Thorp JA et al. (2002) Holocene geochronology of a continental-shelf mudbelt off southwestern Africa. *The Holocene* 12(1): 59–67.

Mucina L and Rutherford MC (2006) *Strelitzia 19: The Vegetation of South Africa, Lesotho and Swaziland*. Pretoria: South African National Biodiversity Institute.

Müller PJ, Kirst G, Ruhland G et al. (1998) Calibration of the alkenone paleotemperature index UK′37 based on core-tops from the eastern South Atlantic and the global ocean (60°N-60°S). *Geochemica et Cosmochimica Acta* 62(10): 1757–1772.

Nelson G and Hutchings L (1983) The Benguela upwelling area. *Progress in Oceanography* 12(3): 333–356.

Nielsen SHH, Koc N and Crosta X (2004) Holocene climate in the Atlantic sector of the Southern Ocean: Controlled by insolation or oceanic circulation? *Geology* 32(4): 317–320.

Olson DB and Evans RH (1986) Rings of the Agulhas current. *Deep Sea Research* 33(1): 27–42.

Pitcher GC and Nelson G (2006) Characteristics of the surface boundary layer important to the development of red tide on the southern Namaqua shelf of the Benguela upwelling system. *Limnology and Oceanography* 51(6): 2660–2674.

Prahl FG and Wakeham SG (1987) Calibration of unsaturation patterns in long-chain ketone compositions for palaeotemperature assessment. *Nature* 330: 367–369.

Prins MA, Bouwer LM, Beets CJ et al. (2002) Ocean circulation and iceberg discharge in the glacial North Atlantic: Inferences from unmixing of sediment size distributions. *Geology* 30: 555–558.

Prospero JM, Ginoux P, Torres O et al. (2002) Environmental characterization of global sources of atmospheric soil dust identified with the NIMBUS 7 Total Ozone Mapping Spectrometer (TOMS) absorbing aerosol product. *Reviews of Geophysics* 40(1): 1–31.

Quick L, Chase BM, Meadows ME et al. (2011) A 19.5kyr vegetation history from the central Cederberg Mountains, South Africa: Palynological evidence from rock hyrax middens. *Palaeogeography, Palaeoclimatology, Palaeoecology* 309(3–4): 253–270.

Reimer PJ, Bard E and Bayliss A (2013) IntCal13 and marine13 radiocarbon age calibration curves 0–50,000 years cal BP. *Radiocarbon* 55(4): 1869–1887.

Renssen H, Goosse H, Fichefet T et al. (2005) Holocene climate evolution in the high-latitude Southern Hemisphere simulated by a coupled atmosphere-sea ice-ocean-vegetation model. *The Holocene* 15(7): 951–964.

Richardson PL, Lutjeharms JRE and Boebel O (2003) Introduction to the 'Inter-ocean exchange around southern Africa'. *Deep Sea Research Part II* 50: 1–12.

Rogers J and Rau A (2006) Surficial sediments of the wave-dominated Orange River Delta and the adjacent continental margin off south-western Africa. *African Journal of Marine Science* 28(3–4): 511–524.

Rommerskirchen F, Eglinton G, Dupont L et al. (2003) A north to south transect of Holocene southeast Atlantic continental margin sediments: Relationship between aerosol transport and compound-specific $\delta13C$ land plant biomarker and pollen records. *Geochemistry, Geophysics, Geosystems* 4(12): 1–29.

Schmid C, Boebel O, Zenk W et al. (2003) Early evolution of an Agulhas Ring. *Deep Sea Research Part II* 50: 141–166.

Schouten M, Ruijter W, van Leeuwen PJ et al. (2000.) Translation, decay and splitting of Agulhas rings in the southeastern Atlantic Ocean. *Journal of Geophysical Research* 105(9): 21913–21925.

Shannon LV and Nelson G (1996) The Benguela: Large scale features and processes and system variability. In: Wefer G, Berger WH, Siedler G et al. (eds) *The South Atlantic: Present and past Circulation*. Berlin: Springer, pp. 163–210.

Shillington FA (1998) The Benguela upwelling system off south-western Africa. *The Sea* 11: 583–604.

Sokolov S and Rintoul SR (2007) On the relationship between fronts of the Antarctic Circumpolar Current and surface chlorophyll concentrations in the Southern Ocean. *Journal of Geophysical Research: Oceans* 112(7): 1–17.

Stager JC, Mayewski PA, White J et al. (2012) Precipitation variability in the winter rainfall zone of South Africa during the last 1400 yr linked to the austral westerlies. *Climate of the past* 8(3): 877–887.

Stewart RH (2009) *Introduction to Physical Oceanography*. College Station, TX: Texas A & M University.

Stuut JBW, Crosta X, van der Borg K et al. (2004) Relationship between Antarctic sea ice and southwest African climate during the late Quaternary. *Geology* 32(10): 909–912.

Toggweiler JR, Russell JL and Carson SR (2006) Midlatitude westerlies, atmospheric CO2, and climate change during the ice ages. *Paleoceanography* 21(2): 1–15.

Tyson PD and Preston-Whyte RA (2000) *The Weather and Climate of Southern Africa* (ed A Attwell). 2nd Edition. Cape Town: Oxford University Press.

Tyson PD, Cooper GRJ and McCarthy TS (2002) Millennial to multi-decadal variability in the climate of southern Africa. *International Journal of Climatology* 22(9): 1105–1117.

Tyson PD, Garstang M and Swap R (1996) Large-scale recirculation of air over southern Africa. *Journal of Applied Meteorology* 35: 2218–2236.

Valsecchi V, Chase BM, Slingsby JA et al. (2013) A high resolution 15,600-year pollen and microcharcoal record from the Cederberg Mountains, South Africa. *Palaeogeography, Palaeoclimatology, Palaeoecology* 387: 6–16.

Vickery KJ, Eckardt FD and Bryant RG (2013) A sub-basin scale dust plume source frequency inventory for southern Africa, 2005–2008. *Geophysical Research Letters* 40(19): 5274–5279.

Weldeab S, Stuut J-BW, Schneider R et al. (2013) Holocene climate variability in the winter rainfall zone of South Africa. *Climate of the past* 9(5): 2347–2364.

Weltje GJ (1997) End-member modeling of compositional data: Numerical-statistical algorithms for solving the explicit mixing problem. *Mathematical Geology* 29(4): 503–549.

Zahn R, Lutjeharms J, Biastoch A et al. (2010) Investigating the global impacts of the Agulhas current. *EOS, Transactions, American Geophysical Union* 91(12): 2009–2010.

Zhao X, Dupont L, Meadows ME et al. (2016.) Pollen distribution in the marine surface sediments of the mudbelt along the west coast of South Africa. *Quaternary International* 404: 44–56.